Surface Temperature from *ERS-1* ATSR Infrared Thermal Satellite Data in Polar Regions

JULIENNE STROEVE

Center for the Study of Earth from Space, Cooperative Institute for Research in Environmental Sciences and Department of Geography, University of Colorado, Boulder, Colorado

MARCEL HAEFLIGER

Department of Geography, Swiss Federal Institute of Technology, Zurich, Switzerland

KONRAD STEFFEN

Center for the Study of Earth from Space, Cooperative Institute for Research in Environmenal Sciences and Department of Geography, University of Colorado, Boulder, Colorado

(Manuscript received 7 July 1995, in final form 4 December 1995)

ABSTRACT

The relationship between Along Track Scanning Radiometer (ATSR) thermal radiances and snow surface temperature for the Greenland ice sheet is examined through forward calculations of the LOWTRAN 7 radiative transfer model. Inputs to the model include in situ radiosonde profile measurements of temperature, pressure and humidity, surface temperatures, and cloud observations for spring–summer 1990 and 1991 from the ETH–CU research camp, located at 69°34′N, 49°18′W on the Greenland ice sheet. Atmospheric correction coefficients were determined through a statistical analysis of daily clear-sky profiles for three different combinations of the ATSR thermal infrared (TIR) channels. Using all available ATSR TIR information, the 11- and 12-μm channels in both the nadir and forward views showed the smallest rms error of less than 0.2 K in the estimated surface temperature. This dual-view algorithm was found to be least sensitive to changes in concentrations of atmospheric constituents, in contrast to the standard "split-window" technique. Assuming accurate surface emissivities can be obtained, the dual-view algorithm is recommended for applications in polar regions where the variety of atmospheric conditions can be large.

1. Introduction

The European Space Agency (ESA) launched the first European Remote Sensing Satellite (*ERS-1*) in July 1991. The platform is in a sun-synchronous orbit with an inclination of 98.52°, providing near complete polar coverage. *ERS-1* carries instrumentation including the Along Track Scanning Radiometer (ATSR), which combines an infrared radiometer and a microwave sounder designed specifically for the measurement of sea surface temperature with an absolute accuracy of 0.5 K, cloud-top temperature, cloud cover, and atmospheric water vapor content. Subsequently, improved accuracy in snow surface temperature estimations, water vapor content, and cloud-cover detection in polar regions should be obtainable with ATSR.

Surface temperature is an important parameter in the estimation of radiative and turbulent heat fluxes from satellite data. In order to estimate radiative fluxes to within 5 W m^{-2}, the surface temperature must be known to an accuracy of less than 1 K (Steffen et al. 1993). Although the surface emitted energy in the infrared window channels is attenuated very little as it passes through the cloud-free polar atmosphere, it can be as large as 3 K during summer. During winter the correction is smaller due to the extremely low moisture content of the winter Arctic atmosphere. A unique feature of the ATSR instrument is that it observes the earth's surface through two views. One through a near-vertical atmospheric path (nadir view) and one at an inclined path (forward view). Assuming that the atmosphere is horizontally stratified and locally stable during the approximately 2 min it takes the satellite subpoint to reach the along-track point, this technique will permit a more accurate atmospheric correction to be determined than previous methods, such as the "split-window" technique (Barton 1985).

In addition, the dual-scan angles enable the ATSR to provide information on atmospheric water vapor content (Gohil et al. 1994). Such data is very sparse in polar regions (e.g., the Greenland ice sheet), consisting of a few point measurements mostly from

Corresponding author address: Dr. Julienne Stroeve, CIRES, University of Colorado, Campus Box 216, Boulder, CO 80309-0216.

coastal stations. Data from the two ATSR swaths can be combined to retrieve accurate water vapor amounts, thereby providing water vapor information for the entire ice sheet.

Another feature of the ATSR instrument that makes it particularly suitable for remote sensing of snow-covered surfaces is the addition of a channel at 1.6 μm. At this wavelength clouds are more reflective than snow-ice-covered surfaces and can be used to distinguish clouds from snow (thereby avoiding contamination of surface temperature retrieval by clouds). This is an advantage over other currently used satellite radiometers such as the Advanced Very High Resolution Radiometer (AVHRR) flown on the NOAA series satellites that currently have no accurate means to differentiate clouds from snow, a problem for Arctic regions that are often covered by clouds.

The purpose of this article is to discuss a means to retrieve accurate surface temperatures in polar regions using the ATSR infrared radiometer. The method is applicable for clear skies only.

2. ATSR—Infrared radiometer

The main sensor characteristics of the infrared radiometer are shown in Table 1. The radiometer uses spectral channels very similar to those flown on recent NOAA meteorological satellites, but with major improvements in accuracy. The radiometer consists of four channels that are fully coregistered, but only three channels are operational at the same time. During the day each pixel contains measurements from channels at 1.6, 11, and 12 μm, and at night from channels at 3.7, 11, and 12 μm. The response functions for the radiometer channels are shown in Fig. 1.

All channels are calibrated on board by incorporating two controlled reference targets (blackbodies) into the instrument scan pattern. A complete description of the advanced technical features of the instrument can be found in European Space Agency (1992).

The scanning mirror of the infrared radiometer provides two views across the subsatellite track. However, due to the conical scan mechanism of the instrument, both the nadir and forward views trace an arc on the earth's surface and the viewing angles change throughout the conical scan. These viewing angles across an ATSR swath can be easily calculated and show that the nadir viewing angle varies from 0° on the ground track to nearly 22° at the edge of the swath. The forward-viewing angle varies between approximately 52° and 56°. The variation of the viewing angle across the ATSR swath is important since the snow surface emissivity, within the atmospheric water vapor window (8–14 μm), is dependent upon viewing angle (Dozier and Warren 1982; Wald 1994). Neglecting the emissivity dependency on viewing angle across the swath leads to temperature errors of 0.1 K for temperatures ranging from 250 to 273 K.

TABLE 1. Infrared radiometer sensor characteristics.

Spectral channels	Four coregistered channels at 1.6, 3.7, 11, 12 μm
IFOV	1 km × 1 km (nadir view), 1.5 km × 2 km (forward view)
Swath width	500 km
Radiometric precision	<0.1 K
SST accuracy	0.5 K over a 50 km × 50 km area with 80% cloud cover

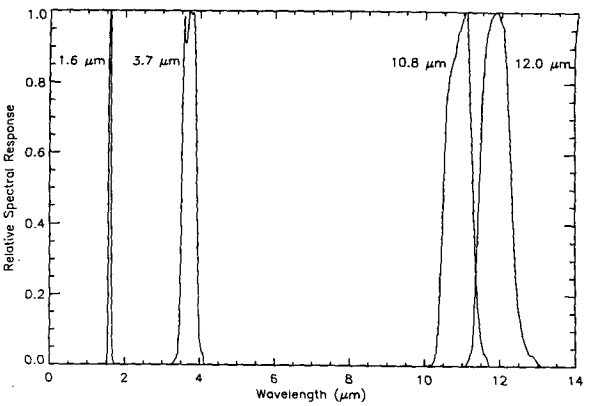

FIG. 1. The relative spectral response of the ATSR 1 channels.

3. Surface temperature retrieval methodology

To retrieve snow surface temperatures from satellite thermal infrared (TIR) data requires 1) a correction for atmospheric absorption and emission due to atmospheric constituents such as water vapor, carbon dioxide, ozone, and aerosols and 2) precise knowledge of the surface emissivity and its angular behavior.

a. Atmospheric correction algorithms

Previous atmospheric correction methods using thermal infrared channels for clear skies in polar regions have used the split-window approach that utilizes measurements at two TIR wavelengths (Haefliger et al. 1993; Key and Haefliger 1992). The accuracy of this algorithm to retrieving snow/ice surface temperatures over the Greenland ice sheet using AVHRR thermal data and sensor scan angle is given as 0.320-K root-mean-square (rms) error (Haefliger et al. 1993). This accuracy value is based on the regression analysis of modeled data only.

Using ATSR data, the surface temperature T_s is expressed using the split-window method as a linear combination of the two nadir infrared channels:

$$T_s = b_0 + b_1 T_{11} + b_2 T_{12}, \quad (1)$$

where T_{11} and T_{12} are the brightness temperatures for the 11- and 12-μm channels, respectively, and the co-

efficients b_0, b_1, and b_2 are obtained from regressing values of T_s, T_{11}, and T_{12}. It can be shown that the constants b_1 and b_2 are related to the atmospheric absorption coefficients in the two channels (k_1 and k_2) so that $b_2/b_1 = -k_1/k_2$. This ratio provides a measure of the relative atmospheric absorption.

In the wavelength regions of the two TIR channels, the difference between the two temperatures measured at different wavelengths for clear skies is primarily a function of the amount of water vapor in the atmosphere. However, the retrieval of surface temperature using this approach is affected by other changes in the atmospheric infrared opacity that occur, for example, with increased concentrations of stratospheric aerosol from volcanic eruptions. This is because although the multiwavelength approach is useful for determining the effects of varying water vapor amounts, it is not sensitive to the effects of other atmospheric constituents, such as aerosols, CO_2, or O_3.

A dual-angle technique can account for absorption variations due to the different concentrations in all absorbing species since it does not depend on the absorptions remaining in proportion as does the split-window technique. It is in this regard that the dual-angle capability of ATSR is expected to give a significant improvement in surface temperature accuracy. To derive the dual-angle algorithm, we make the same assumptions as used in the split-window method. Namely, we assume the atmospheric optical depth $\tau = kX$, where X is the total absorber column content and k is the absorption coefficient, so that we can approximate the atmospheric transmittance by $T = 1 - kX$. This assumption is valid for areas of weak absorption, which occurs between the widely spaced lines in the atmospheric window region (8–14 μm). Making a Taylor series expansion of the blackbody function at surface temperature T_s together with the above expression for the atmospheric transmittance allows the radiative transfer equation to be written as

$$T_s = T(\theta_1) + \left(\frac{-a_1}{a_1 - a_2}\right)[T(\theta_1) - T(\theta_2)], \quad (2)$$

where $a_1 = \sec(\theta_1)$, $a_2 = \sec(\theta_2)$, and $\theta_{1,2}$ is the scanning angle for the nadir and forward views, respectively.

Using this relationship the atmospheric absorption is only dependent upon the two different pathlengths rather than dependent on wavelength, and therefore, independent of the nature of the absorber. Equation (2) states that the difference between the temperature measured at nadir and that measured in the forward view, when added to the nadir value, gives an estimate of the surface temperature corrected for atmospheric absorption and emission. In reality, the difference between the two temperatures at different viewing angles will slightly underestimate the contribution of the atmosphere since the optical depth varies more like kX^b, where $b < 1$. Therefore, we rewrite (2) as

$$T_s = b_0 + b_1 T(\theta_1) + b_2\left(\frac{-a_1}{a_1 - a_2}\right)[T(\theta_1) - T(\theta_2)], \quad (3)$$

where again the coefficients b_0, b_1, and b_2 are obtained from a multiple linear regression of the surface temperature and satellite brightness temperatures. In the following discussions, this equation is referred to as the dual-view algorithm for one channel (11 μm) (DV1C).

Alternatively, we also consider a multichannel and multiview algorithm where the surface temperature is computed as a linear combination of all the thermal infrared data available, that is, the 11- and 12-μm channels in both views:

$$T_s = b_0 + b_1 T_{11n} + b_2 T_{11f} + b_3 T_{12n} + b_4 T_{12f}, \quad (4)$$

where n and f denote the nadir and forward views, respectively. This equation is referred to as the dual-view algorithm in both TIR channels (DV2C).

b. *Simulation of ATSR data*

Due to the lack of sufficient surface temperature data during the 1992 validation period, the brightness temperatures have to be modeled. The radiances of the ATSR thermal channels were simulated using the LOWTRAN 7 radiative transfer code. Input data were pressure, temperature, and humidity profiles derived by radiosonde ascents at the research camp on the Greenland ice sheet (69°34′N, 49°18′W). The camp was established by the Swiss Federal Institute of Technology (ETH) and is currently operated by the University of Colorado (CU) and now referred to as the ETH–CU camp. These profiles were collected during summer months (June–August) in 1990 and 1991 and have column water vapor amounts ranging from 1.52 to 8.75 kg m^{-2}. Above the highest radiosonde level, standard values for stratospheric temperature profiles were used. Only situations with less the three-eighths cloud cover were used in the analysis, consisting of a total of 90 profiles. Sensitivity studies have shown that thermal radiances are not influenced by clouds up to this amount.

Tropospheric extinction with a visibility of 50 km was assumed together with standard summer profiles for both the tropospheric and stratospheric aerosols. Ozone has a strong absorption band at 9.6 μm, but the strength of the absorption lines decreases rapidly with increasing wavelength. Although the absorption by O_3 is weak in both the 11- and 12-μm channels, a 15% change in ozone concentration leads to temperature errors as large as 0.1 K for temperatures ranging from 250 to 273 K. However, since no information on O_3 concentrations were available, standard subarctic O_3 model concentrations were assumed.

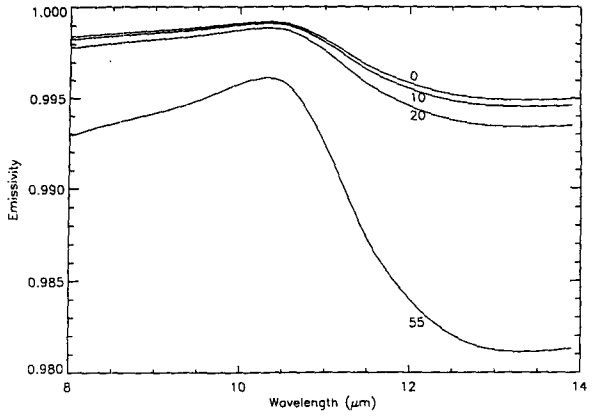

FIG. 2. Directional emissivity of snow at crystal grain size of 300 μm (diameter) for viewing angles of 0°, 10°, 20°, and 55°.

Surface temperatures were calculated after the Stefan–Boltzmann law ($L = \sigma T_s^4$) using measured outgoing longwave radiation at the camp and assuming the snow surface is a blackbody. Since the uncertainty of the surface radiation measurements is given as 3% this amount was added and subtracted, respectively, to each measured value. This way two additional profiles were created for every original clear-sky profile, which differ only by different surface temperatures. This results in a sample size of 270 clear-sky profiles, with surface temperatures ranging from 252.34 to 273.15 K.

To take into account more realistic atmospheres, such as winter concentrations of atmospheric constituents (i.e., ozone) or high stratospheric aerosol loadings due to volcanic eruptions, the LOWTRAN 7 model was run again. The first run consisted of including a moderate volcanic profile with aged volcanic extinction to simulate the possibility of volcanic aerosols present in the stratosphere. Aerosol loading in the arctic atmosphere also varies seasonally, with higher concentrations occurring during the winter (Djupstrom et al. 1993). In the next model run the summer aerosol profile was replaced by a winter aerosol profile. Finally, the model was run for the fall–winter conditions to study the effects of minimum Arctic ozone concentration.

As mentioned previously, the sensor scanning angle is not constant but varies across the ATSR swath. Therefore, six viewing angles were chosen to simulate the satellite brightness temperatures: five angles for the nadir view—0°, 5°, 10°, 15°, and 20°—and one angle for the forward view—55°. For each viewing angle the spectral emittance of snow is also needed for input in LOWTRAN 7 and was calculated as described in the following section.

c. *Surface emissivity*

In general, snow surface emissivity is dependent upon snow pack characteristics (i.e., density, liquid water, and grain size) and the viewing angle. Previous work by Dozier and Warren (1982) found the emissivity to be insensitive to grain size as well as the liquid water content and density of the snowpack. More recent work by Salisbury et al. (1994), however, found snow grain size and packing fraction to be important, causing snow emissivity to be as low as 0.95 at 13 μm for coarse granular snow (grain size from 1 to 2 mm in diameter). This can result in temperature measurements at nadir to be in error by as much as 3 K (Wald 1994). In regards to the ATSR thermal channels, using the 11-μm channel would result in a temperature difference of 0.62 K using the emissivity as calculated by Dozier and Warren (1982) to that for coarse granular snow measured by Salisbury et al. (1994). If the 12-μm channel is used, the error in derived temperature is 1.08 K.

TABLE 2. Angular emissivities of snow for ATSR TIR channels.

Scan angle	11-μm channel	12-μm channel
0°	0.9984	0.9960
5°	0.9984	0.9959
10°	0.9983	0.9957
15°	0.9981	0.9953
20°	0.9978	0.9947
55°	0.9931	0.9845

During summer in central Greenland, coarse-grained, surface hoar layers may form with grains sizes at the centimeter scale (Shuman and Alley 1993). However, excluding hoar formation, grain sizes over the Greenland ice do not vary much. This is due to

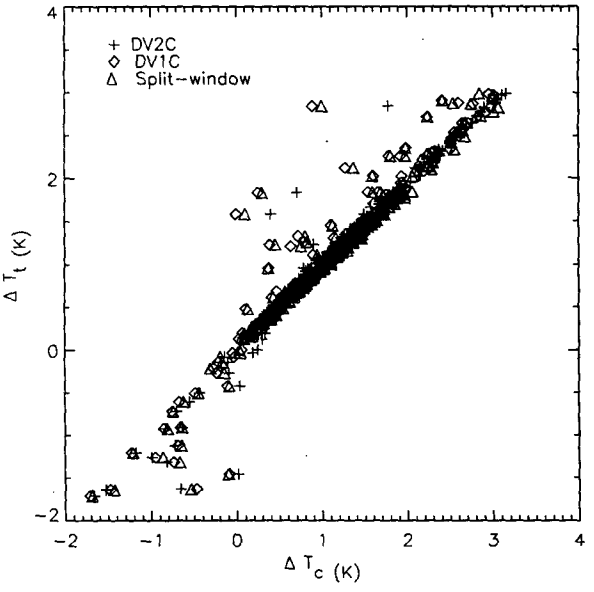

FIG. 3. Computed atmospheric correction ΔT_c versus the true atmospheric correction ΔT_t for the three algorithms.

constant wind-transported snow that has grain sizes on the order of 0.3–0.5 mm. Therefore, except during periods of depth hoar events in the summit region, a constant grain size can be assumed.

At the wavelengths of TIR channels, angular effects on emissivity have been found to be much greater than snow grain size or packing effects for naturally occurring snow (Wald 1994). In regards to the ATSR viewing angles, failure to account for the effect of viewing angle can lead to temperature errors as large as 1 K. Directional surface emissivities for snow were therefore modeled following the procedure outlined in Dozier and Warren (1982) where the single-scattering albedo and asymmetry parameter were calculated from the Mie equations, and the directional, wavelength-dependent emissivities were derived from the delta-Eddington approximation to the radiative transfer equation. Figure 2 shows the directional emissivity of snow $\epsilon_s(\lambda, \theta)$ for viewing angles (θ) relevant to the ATSR scanning geometry.

Directional emissivities were then integrated with the response functions for each TIR channel to obtain a wavelength-integrated emissivity of snow

$$\epsilon_i(\theta) = \frac{\int_{\lambda_1}^{\lambda_2} \epsilon(\lambda, \theta) S_i(\lambda) d\lambda}{\int_{\lambda_1}^{\lambda_2} S_i(\lambda) d\lambda}, \qquad (5)$$

where $\epsilon(\lambda, \theta)$ is the emissivity in viewing direction θ at wavelength λ and S is the sensor response function that is 0 outside of $[\lambda_1, \lambda_2]$. These emissivities are given in Table 2 as a function of viewing angle for the ATSR TIR channels.

4. Results

a. Algorithm comparisons

Figure 3 shows the result of the initial LOWTRAN 7 model run, where standard summer tropospheric aerosols and subarctic summer atmosphere were assumed. Plotted is the calculated atmospheric correction for the nadir view at 11-μm ΔT_c, [$\Delta T_c = T_s$(computed) $- T_{11n}$] versus the true atmospheric correction ΔT_t, [$\Delta T_t = T_s$(measured) $- T_{11n}$] for each of the three different algorithms. The coefficients b_0–b_4 are shown in Table 3 along with the rms (standard deviation of the residuals). In Table 3 and in the following discussions, case I refers to the initial model run, case II includes the volcanic aerosols, case III is the winter aerosol run, and case IV represents the winter subarctic atmosphere. We find that for case I the split-window algorithm in the nadir scan gives a snow surface accuracy of 0.257 K, which is a slight improvement over the AVHRR equivalent algorithm. This accuracy value is based on the regression analysis of the modeled data only; it does not include other errors such as measurement error, emissivity error, or unmodeled atmospheric effects. The DV1C algorithm gives an accuracy of 0.265 K. There is, therefore, no apparent advantage in using the DV1C algorithm over the conventional split-window algorithm.

Similar results are found for the other three cases. This is because the only atmospheric variations in each case are the tropospheric temperature and water vapor profiles, while the aerosol distributions and atmospheric constituents such as O_3 and CO_2 remained constant. Previous estimations of sea surface temperature (SST) using the split-window technique have shown, for example, that major changes in stratospheric aerosol content require modifications of operational SST al-

TABLE 3. Surface temperature retrieval coefficients for the four individual model case runs. Case I is the initial model run, case II includes volcanic aerosols, case III refers to the winter aerosol model run, and case IV represents the winter subarctic atmosphere.

Algorithm	b_0	b_1	b_2	b_3	b_4	rms (K)
Case I						
Split-window	1.15	3.51	−2.51	—	—	0.257
DV1C	−1.67	1.01	1.33	—	—	0.265
DV2C	1.73	5.47	−2.64	−3.57	1.73	0.188
Case II						
Split-window	6.60	3.12	−2.12	—	—	0.239
DV1C	0.50	1.00	1.33	—	—	0.250
DV2C	2.02	4.95	−4.38	−1.30	1.72	0.175
Case III						
Split-window	6.75	3.12	−2.12	—	—	0.238
DV1C	0.46	1.00	1.33	—	—	0.250
DV2C	2.98	4.93	−4.30	−1.34	1.70	0.175
Case IV						
Split-window	6.70	3.12	−2.12	—	—	0.238
DV1C	0.45	1.00	1.33	—	—	0.250
DV2C	0.67	4.94	−4.36	−1.30	1.71	0.177

TABLE 4. Surface temperature retrieval coefficients for all cases combined.

Algorithm	b_0	b_1	b_2	b_3	b_4	rms (K)
Split-window	−12.13	0.70	0.36	—	—	1.056
DV1C	8.21	0.97	1.39	—	—	0.720
DV2C	0.50	4.87	−4.85	−0.78	1.76	0.185

gorithms (Walton 1985). It is for variable atmospheric conditions that the DV1C algorithm is expected to give a higher accuracy in surface temperature retrieval than the split-window method.

Although, the model accuracies are similar for the split-window and DV1C algorithms, we do observe that the effect of the change in atmospheric absorption from the initial model run (case I) is greater for the split-window algorithm than for the DV1C algorithm. This is observed by comparing the ratios of b_2/b_1 for each method (comparing the relative atmospheric absorption). For the split-window algorithm, the absolute value of b_2/b_1 is 0.715 for case I and decreases by 0.035 for the other three cases. For the DV1C algorithm the change is only 0.013. A change of 0.035 is equivalent to a temperature discrepancy of about 0.4 K across a range of surface temperatures from 252 to 273 K, while a change of 0.013 is equivalent to a difference of only 0.2 K.

For all four cases, using both the 11- and 12-μm channels and both the nadir and forward views results in the smallest error in snow surface temperature estimation; accuracy of 0.175 to 0.188 K. This suggests that the DV2C algorithm, which uses both TIR channels, will give a more accurate estimation of the surface temperature.

To simulate a more realistic atmosphere, we combine the above four cases and recompute the surface temperature retrieval coefficients. These coefficients are given in Table 4 for the three different algorithms. Now the DV1C algorithm shows a significant increase in surface temperature accuracy over the split-window method. However, both methods, the split-window and DV1C, perform rather poorly. This is due to the variability of atmospheric conditions that is the dominant source of error for both these algorithms. In contrast, the DV2C method still gives a similar accuracy as for the individual cases, illustrating that this model is the least dependent on the model assumptions and the varying atmospheric conditions.

For comparison, Bamber and Harris (1994) used an equation similar to the DV1C to derive surface temperatures using sounding data from six stations in Antarctica. They give an accuracy of 0.015 K in surface temperature retrieval. They, however, did not vary any atmospheric constituents in their calculations. Aerosols in particular become important in the Arctic during winter "haze" events.

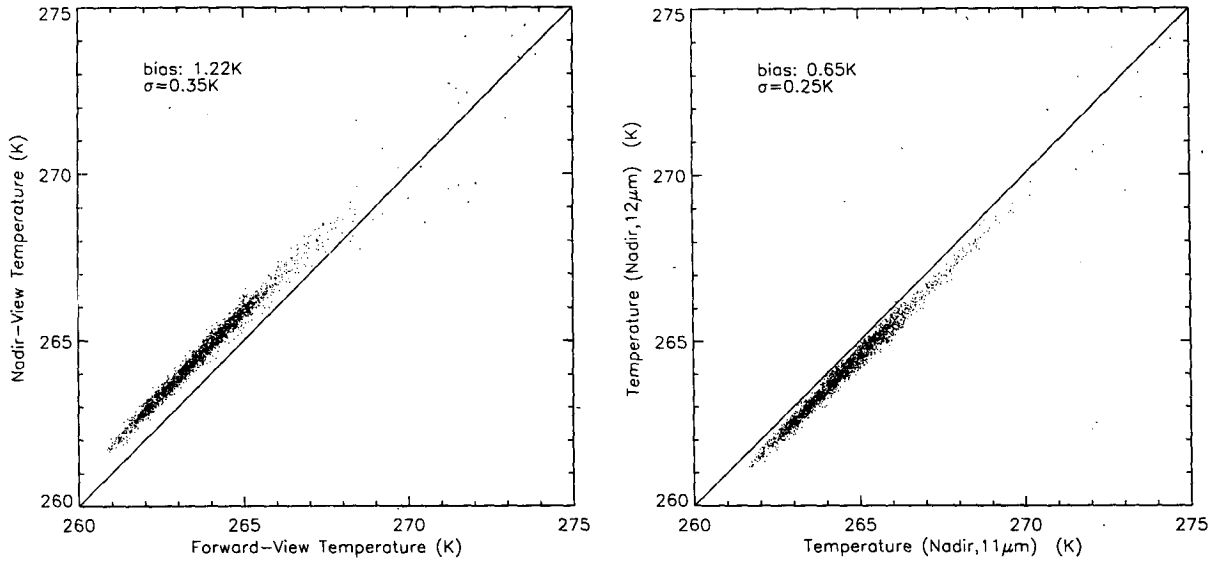

FIG. 4. (a) 19 June 1992: comparison of the satellite brightness temperatures in the 11-μm channel for nadir and forward views for a 25 km × 25 km grid centered around 69°34′N, 49°18′W. (b) 19 June 1992: comparison of the satellite brightness temperatures measured at nadir in the 11- and 12-μm channels for a 25 km × 25 km grid centered around 69°34′N, 49°18′W.

b. Application to an ATSR scene

Before applying a surface temperature retrieval algorithm, it is necessary to verify that the initial ATSR images actually have different brightness temperatures, either because of the different viewing angles or the different channels used. Figure 4a shows the comparison on a pixel basis between brightness temperatures measured at 11 μm on the nadir scan with those measured on the forward scan. Figure 4b compares the brightness temperatures measured at 11 μm with those measured at 12 μm for the nadir view. Both figures show brightness temperatures acquired 1506 UTC 19 June 1992 for a 25 km $\times$ 25 km grid centered around the ETH–CU camp on the Greenland ice sheet (69°34′N, 49°18′W). Brightness temperatures measured on the nadir view are typically found to be greater than those measured on the forward view. This is because there is less atmosphere to travel through when viewing the surface at nadir and also because the mean atmospheric temperature T_a is generally less than the surface temperature T_s. The temperatures at 11 μm are also generally greater than those found at 12 μm because the atmosphere is more transparent at 11 μm than at 12 μm.

There are a few points where the forward-view brightness temperatures are greater than the nadir-view brightness temperatures. These points occur near the edge of the ice sheet, where terrain and more sudden temperature variations occur, causing the different ground resolutions of the two views to become important. This is also the reason why points appear more scattered on this graph than on the graph comparing the two TIR nadir channels.

Figure 5 shows the application of the DV2C model in calculating the surface temperature for 19 June 1992. The image shows the western coast of the Greenland ice sheet near Disko Island between 68°29′ and 74°41′N. Over the ice sheet the surface temperatures are relatively cold, with temperatures ranging from about 250 to 273 K, where the warmer temperatures are found along the coast. Thus, on this summer day there is no melting of the snow/ice in this region. This is consistent with passive microwave observations that also show no melt on this day (Abdalati 1995, personal communication). A few clouds are detected on the ice

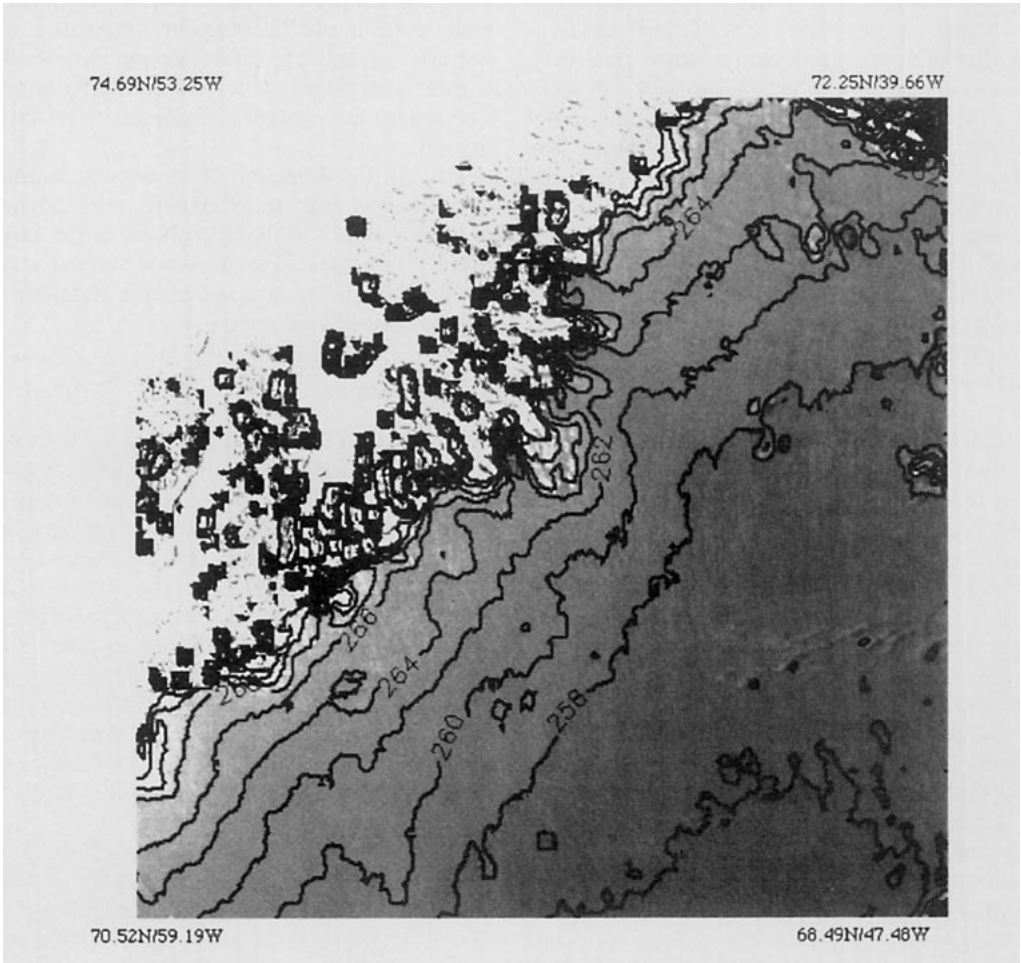

FIG. 5. Calculated surface temperature on the Greenland ice sheet for 19 June 1992. The image shows the western coast of the Greenland ice sheet near Disko Island.

sheet in the upper and lower right-hand corners of the image, as well as a few in the lower left-hand corner. Unfortunately, we have no surface temperature data with which to verify these results.

5. Accuracy of the surface temperature retrieval

A major source of error in the surface temperature retrieval coefficients is a direct result of modeling the atmospheric absorption. Comparisons between theoretical and experimental SST algorithms have shown that it is still not possible to accurately model the atmospheric absorption in the ATSR TIR channels (Barton 1992). This is due largely to an uncertainty in the strength of the water vapor continuum absorption used in the atmospheric model. The result of this uncertainty is a need to fine tune the model with in situ data. However, in the polar regions where the atmosphere has a relatively low atmospheric water vapor content, the errors in estimated brightness temperatures are predicted to be small.

Another source of error is the difference in the "true" atmospheric conditions from the conditions used as input into the LOWTRAN 7 model. We still have a only a limited knowledge of the spatial and temporal variability of atmospheric temperature, humidity, and aerosols. This error will be greatest for the split-window algorithm since the ratio of absorption will not remain constant and least for the DV2C algorithm. The use of only one station data for the temperature and humidity profiles, which was only available for the spring–summer season, affects the algorithm coefficients as well. Future efforts will include incorporating other Greenland station data into the model runs to determine the magnitude of this error.

Errors in surface emissivity probably contribute the largest errors in the retrieved surface temperature. As mentioned previously, grain size is found to be important. Since changes in grain size affect the 12-μm channel the greatest, using an algorithm that incorporates this channel will lead to larger errors in surface temperature. As per the coefficients in Table 4, assuming the modeled temperatures are in error by 0.62 K (at 11 μm) and 1.08 K (at 12 μm), using the DV2C algorithm will result in a change of about 1 K in surface temperature. Using the DV1C algorithm will only result in change of about 0.6 K. To investigate the error due to errors in modeling the directional surface emissivity, surface emissivities were changed by 0.002. For comparison, Wald (1994) found their model to disagree with Dozier and Warren's model by about 1% at low incidence angles. At high incidence angles the two models gave virtually identical results. A 0.002 variability in snow emissivity results in a change in modeled brightness temperatures of approximately 0.06–0.28 K. A 0.28-K error in the 12-μm oblique view data using the DV2C algorithm will lead to a error of about 0.5 K in surface temperature. Using the DV1C algorithm, the error is 0.19 K. Therefore, to use the 12-μm data in an atmospheric correction requires very accurate surface emissivities. To obtain snow surface temperatures to an accuracy of 0.1 K will require the surface emissivity to be known to within 0.1%.

In addition, since emissivity is strongly dependent on viewing angle, local slope and instrument viewing can combine to give large effective viewing angles. Fortunately, over the Greenland ice sheet, surface undulations are of the order of 50 m for every 5 km and do not significantly affect the viewing angle. In regions with large topographic variations, however, this could become important. It is also important to consider emissivity variations due to surface heterogeneity. Unlike sea ice and land areas, the snow types of the Greenland ice sheet extend over several tens of kilometers at a minimum. Over sea ice the emissivity will be dependent upon the exact mixture of ice of various thicknesses, open water, and snow cover.

Caution must also be taken when comparing measurements from two different spatial scales. Over a fairly homogeneous surface such as the Greenland or the Antarctic ice sheet this error will be small. However, combining a larger forward pixel with a smaller nadir pixel could become important over sea ice, especially during the melt season where the surface within each pixel is likely to be highly heterogeneous. The magnitude of this error needs to be further investigated.

Finally, the detection of clouds, including subvisual cirrus, is necessary to avoid contaminated pixels. Cloud detection is still a major problem in the polar regions. Methods of cloud detection over snow/ice surfaces using the 1.6-μm channel together with the thermal channels is currently in progress.

6. Conclusions

The LOWTRAN 7 model was used to derive coefficients for three different snow surface temperature retrieval algorithms. Apart from system noise, the accuracy of snow surface temperature retrieval is degraded by the variability in atmospheric conditions such as water vapor and aerosols. It was shown that using all available thermal infrared data from the ATSR instrument will give the greatest accuracy in snow surface temperature. In terms of modeled accuracy only, the DV2C algorithm can retrieve snow surface temperature to within 0.2 K. Modeling results also show the DV2C algorithm to be the least sensitive to any errors in the retrieval coefficients due to varying atmospheric conditions.

The accuracy in snow surface estimation from satellite infrared radiometers is largely dependent upon accurate surface emissivities. Variations in grain size and effective viewing angle can combine to give large errors in surface temperature. Fortunately over the Greenland ice sheet, topographic variations do not sig-

nificantly effect the viewing angle and constant wind-driven snow result in relatively homogeneous snow grain sizes. In regions where these factors do become important, it might be necessary to exclude the 12-μm channel from any atmospheric correction scheme.

As with the previously developed AVHRR algorithms, some fine tuning with in situ data will probably be needed. This is because the absorption due to atmospheric water vapor at infrared wavelengths is still not well understood. Surface temperature data collected at the ETH–CU camp during the spring–summer seasons in 1993 and 1994 will provide the necessary validation data.

Although the total radiances in the window channels are primarily dependent upon the surface temperature, they also have a secondary dependence on water vapor as the channels are not absolutely transparent. Barton et al. (1989) showed a slight increase in sea surface temperature estimation when atmospheric water vapor was included in the surface temperature prediction. However, due to the low water vapor content of polar atmospheres, incorporating independent atmospheric water vapor measurements into the retrieval algorithms might not significantly improve snow surface temperature estimation. This needs to be further investigated.

Acknowledgments. This work was supported under contract NAGW-2158 by NASA Ocean Science Branch, by the Swiss Federal Institute of Technology (ETH), Zurich (0-43-018-91), and the Swiss National Foundation for Scientific Research (20-32649-91). *ERS-1* ATSR satellite data was provided by the Rutherford Appleton Laboratory.

REFERENCES

Bamber, J. L., and A. R. Harris, 1994: The atmospheric correction for satellite infrared radiometer data in polar regions. *Geophys. Res. Lett.*, **21,** 2111–2114.

Barton, I. J., 1992: Satellite-derived sea surface temperatures—A comparison between operational, theoretical, and experimental algorithms. *J. Appl. Meteor.*, **31,** 433–442.

——, A. M. Zavody, D. M. O'Brien, D. R. Cutten, R. W. Saunders, and D. T. Llewellyn-Jones, 1989: Theoretical algorithms for satellite-derived sea surface temperature. *J. Geophys. Res.*, **94**(D3), 3365–3375.

Barton, T., 1985: Transmission model and ground truth investigation of satellite derived sea surface temperature. *J. Climate Appl. Meteor.*, **24,** 508–516.

Djupstrom, M., J. M. Pacyna, W. Maenhaut, J. W. Winchester, S. M. Li, and G. E. Shaw, 1993: Contamination of arctic air at three sites during a haze event in late winter 1986. *Atmos. Environ.*, **27A,** 2999–3010.

Dozier, J., and S. G. Warren, 1982: Effect of viewing angle on the infrared brightness temperature of snow. *Water Resour. Res.*, **18,** 1424–1434.

European Space Agency, 1992: ERS-1 system manual ESA SP-1146, 3–87.

Gohil, B. S., A. K. Mathur, and P. C. Panday, 1994: An algorithm for sea surface temperature estimation from ERS-1 ATSR using moisture dependent coefficients: A simulation study. *Int. J. Remote Sens.*, **15,** 1161–1167.

Haefliger, M., K. Steffen, and C. Fowler, 1993: AVHRR surface temperature and narrow-band albedo comparison with ground measurements for the Greenland ice sheet. *Ann. Glaciol.*, **17,** 49–54.

Key, J., and M. Haefliger, 1992: Arctic ice surface temperature retrieval from AVHRR thermal channels. *J. Geophys. Res.*, **97**(D5), 5885–5893.

Salisbury, J. W., D. M. D'Aria, and A. Wald, 1994: Measurements of thermal infrared spectral reflectance of frost, snow, and ice. *J. Geophys. Res.*, **99,** 24 235–24 240.

Shuman, C., and R. Alley, 1993: Spatial and temporal characterization of hoar formation in central Greenland using SSM/I brightness temperatures. *Geophys. Res. Lett.*, **20,** 2643–2646.

Steffen, K., and Coauthors, 1993: Snow and ice applications of AVHRR in polar regions: Report of a workshop held in Boulder, Colorado, 20 May 1992. *Ann. Glaciol.*, **17,** 1–16.

Wald, A., 1994: Modeling thermal infrared (2–14 μm) reflectance spectra of frost and snow. *J. Geophys. Res.*, **99,** 24 241–24 250.

Walton, C., 1985: Satellite measurement of sea surface temperature in the presence of volcanic aerosols. *J. Climate Appl. Meteor.*, **24,** 501–507.